

On the Use of Structural Vibrations to Release Stiction Failed MEMS

Amit A. Savkar, Kevin D. Murphy, Zayd C. Leseman, *Member, IEEE, Student Member, ASME*, Thomas J. Mackin, *Member, IEEE, Member, ASME*, and Matthew R. Begley

Abstract—This paper identifies dynamic excitation parameters that promote decohesion of stiction-failed microcantilevers. The dynamic response of “s-shaped” adhered beams subjected to harmonic loading is described using modal analysis; this model is then used to predict the onset of debonding in the context of a critical interface energy. These theoretical results are used to rationalize preliminary experiments, which illustrate that dynamic excitation may be used to affect partial or complete repair of stiction-failed microcantilevers. The theoretical results provide fundamental insight regarding regimes where resonant effects trigger debonding and can serve as a potential mechanism for stiction repair. The models illustrate that driving a structure at resonance is usually beneficial with regards to debonding. However, this is not universally true; there is no benefit to driving a device at frequencies with unfavorable mode-shapes. Thus, these results provide a reasonable physical and mathematical explanation for the preliminary experimental results, while providing a roadmap for identifying parameters in future tests. [2006-0055]

Index Terms—Repair, stiction failure, vibrations.

I. INTRODUCTION

MICROELECTROMECHANICAL systems (MEMS) are continually plagued by reliability issues arising from adhesion between adjacent components, which is known to promote wear and operational failures. In extreme circumstances, the adhesion is large enough to prevent separation, a phenomenon commonly referred to as *stiction-failure*. There are a variety of physical mechanisms that promote adhesion, including capillary effects (often promoted by hydroxyl groups introduced during the release procedure), van der Waals forces, and electrostatic forces [1], [2].

Consider, for example, the stuck microcantilever shown in Fig. 1(a). Here an initially freestanding cantilever is stuck to the substrate in what is commonly referred to as the “s-shape.” The strain energy in the deformed structure serves as a driving force for decohesion. The competition between stored elastic energy and adhesive forces at the contact interface has naturally led to

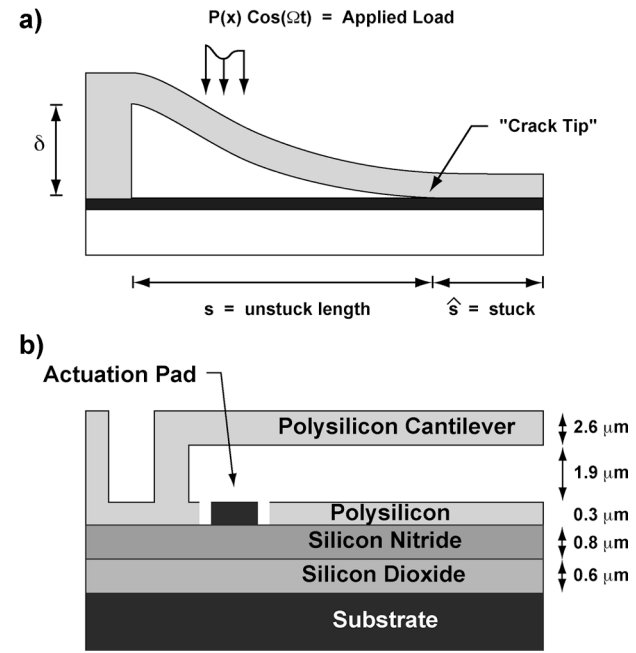


Fig. 1. (a) A schematic of a stiction-failed s-shaped beam. (b) A schematic of the material geometry of the beam/substrate used in the preliminary tests.

the application of fracture mechanics models. These models introduce a critical interface adhesion energy that must be overcome to initiate debonding [3]–[8]. This framework is attractive because of both its simplicity (i.e., it does not require an explicit description of a force-separation adhesion relation) and its ability to predict failure using a single parameter characterizing the interface, regardless of the physical mechanism underlying the adhesion. This is a critical advantage since many adhesion mechanisms involve nanoscale forces and displacements that are difficult to measure directly.

The principal motivation for this analysis is to evaluate the efficacy of using structural vibrations to promote the release of adhered structures. Such vibrations can often be induced using the functionality of the MEMS device itself, which is a key advantage over alternative approaches that require additional instrumentation for external excitation (e.g., ultrasonic substrate pulses, laser heating, etc.). To enhance the efficiency of structural vibrations to trigger stiction repair, one may combine vibrations with surface treatments, such as hydrogen terminating treatments, self-assembly monolayers, fluorocarbon films formed by plasma polymerization reactions, and diamond-like carbon coatings [9], [10].

Manuscript received April 11, 2006; revised August 15, 2006. Subject Editor E. Obermeier.

A. A. Savkar and K. D. Murphy are with the Department of Mechanical Engineering, University of Connecticut, Storrs, CT 06269-3139 USA (e-mail: asavkar@engr.uconn.edu; kdm@engr.uconn.edu).

Z. C. Leseman is with the Department of Mechanical Engineering, The University of New Mexico, Albuquerque, NM 87131 USA (e-mail: zleseman@gmail.com).

T. J. Mackin is with the Department of Mechanical Engineering, California Polytechnic State University, San Luis Obispo, CA 93407 USA (e-mail: tmackin@calpoly.edu).

M. R. Begley is with the Department of Civil Engineering and Department of Material Science and Engineering, University of Virginia, Charlottesville, VA 22904-4742 USA (e-mail: begley@virginia.edu).

Digital Object Identifier 10.1109/JMEMS.2006.885986

Previous attempts have been made to promote stick-release by delivering ultrasonic pulses (waves) through the substrate to the stiction-failed component [9], [10]. This purely experimental effort achieved some measure of success. However, this approach is not specific to the failed component, in that neighboring (nonstuck) components are also subjected to excitation. Another approach that has received considerable attention involves applying short laser pulses to repair the component thermally [13]–[16]. In contrast to the wave propagation approach, laser pulse heating is component specific. Again, structural vibrations could be used to compliment this existing approach. Vibrations could be combined with laser pulse heating; the increase in strain energy resulting from laser heating can be supplemented with dynamic energy imparted via vibrations, leading to highly effective repairs. In the event the laser heating produces sufficient thermal stresses to cause component buckling, dramatic snap-through vibrations could promote significant out-of-plane deformation, leading to debonding [16].

This paper begins by describing some preliminary experimental results, which clearly demonstrate that electrically induced vibrations can achieve partial or total repair of a stiction-failed microcantilever. These observations provide the motivation to develop a vibrations/fracture mechanics model to predict the effect of the structural dynamic response on debond *initiation*, such that effective parameter combinations can be estimated a priori. The models presented here couple the dynamic response of the beam (as predicted via modal analysis) to a fracture mechanics model used to predict growth of the unstuck region; see Fig. 1(a). The important end result is an analytical expression for the energy release rate in terms of the dynamic response of the beam. Of course, the energy release rate reduces to previously published quasi-static results in the limit that the excitation frequency goes to zero [3]–[8].

A linear vibration model is developed to predict the time dependent response of a partially adhered beam, as shown in Fig. 1(a). This model superposes a closed-form solution for the dynamic response of a clamped-clamped beam of length s (the free length of the beam) with the static solution, describing the initial s-shape. It should be emphasized that the vibration analysis is only valid for a beam of fixed unstuck length. After decohesion is initiated and the beam begins to peel away from the substrate, the unstuck length changes and the vibration analysis is no longer valid. Hence, this paper focuses only on the *initiation* of debonding.

These models are used to determine parameter combinations that lead to the initiation of decohesion in microcantilevers. Particular attention is paid to the role of the forcing amplitude (P) and the forcing frequency (Ω) in decohesion. This leads to well-defined regions in the (Ω, P) parameter space where vibrations are effective in initiating peeling. Other combinations exist where vibrations are less effective. These various behaviors form a rational basis for choosing excitation parameters for initiating release of stiction-failed microcantilevers and are explained in terms of the underlying physics of the system.

II. VIABILITY OF THIS APPROACH—PRELIMINARY EXPERIMENTS

To demonstrate the potential use of structural vibrations to produce stiction-repair, preliminary experiments were carried

out on stiction-failed microcantilevers. The tests involved s-shaped and arc-shaped stiction-failed microcantilevers that were driven using electrostatic forces. A schematic cross-sectional view of the microcantilevers is shown in Fig. 1(b). All beams considered in this work have a free length of $1000 \mu\text{m}$ and a width of $30 \mu\text{m}$. Other relevant dimensions are shown in Fig. 1(b). Two layers of dielectric materials (silicon dioxide and silicon nitride) serve as electrical insulation between the silicon substrate and polysilicon cantilevered beams. During electrical actuation, the doped cantilevered beams were electrically grounded while a varying voltage was applied to the actuation pad. The microcantilever arrays were fabricated at Sandia National Laboratories using the four-layer SUMMiT IV process [17].

Release of the microcantilevers was performed at the experimental site. The die was received from Sandia with the sacrificial layers intact. These layers were then removed using a 15 min etch in a solution of 49% HF. The die was then rinsed using deionized water and subsequently rinsed in isopropyl alcohol. The duration of all rinses was 5 min. Following the isopropyl alcohol rinse, the die was placed onto a hot plate at 110°C for 10 min. The die used in these experiments were then stored in a desiccator for several months.

Fig. 2 shows deflection profiles of a set of beams in two different configurations: s-shaped and arc-shaped (stuck at the tip). These profiles were determined using a Michelson interferometer [7], [8], [16], [18]. Initially [Fig. 2(a)], the beam was in the s-shape. In the first set of experiments, oscillations were induced in the beam by applying a square wave voltage to the actuator pad at an amplitude of 20 V peak-to-peak. The frequency of the square wave was swept from 20.6 MHz down to 4 MHz, at a rate of approximately 200 kHz/s, and the geometry changed from s-shaped to arc-shaped; see Fig. 2(b). This experiment was repeated three times with the same set of beams, with each result being the same. An array of beams can be repeatedly used by applying a 100 VDC to the actuation pad causing the beams to repeatedly fail in an s-shaped mode.

In a second set of experiments, arc-shaped beams were subjected to a sinusoidal excitation with a peak-to-peak amplitude of 220 V, while the frequency was swept from 2.6 to 400 kHz at an approximate rate of 4 kHz/s. This resulted in complete repair of two of the six initially arc-shaped beams, producing freestanding beam shapes; see Fig. 3.

The beams in both sets of experiments were observed to oscillate with the applied voltage. These oscillations appeared to correspond to the frequency of excitation. Increasing the excitation frequency caused increased oscillations in the beam, and the opposite was observed for decreasing the excitation frequency. The correspondence between the driving and response frequency was not quantified due to the experimental equipment utilized (an interferometric microscope with no additional instrumentation). It is interesting to note that the direction of the frequency sweeps leads to dramatically different behavior; a rationale for this behavior is provided in the discussion.

These proof-of-concept tests clearly demonstrate that it is possible to repair stiction-failed cantilevers using structural vibrations. More detailed experiments are being conducted to characterize more fully the efficiency of this repair strategy

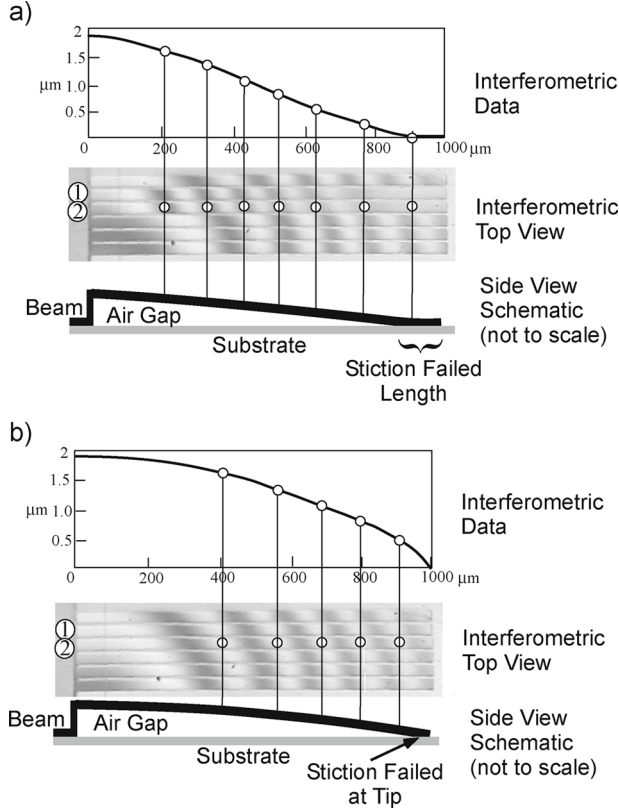


Fig. 2. (a) and (b) show the same set of beams in different configurations. The out-of-plane displacements of the beams are determined using a Michelson interferometer, where two adjacent similarly colored fringes are 274 nm apart. (a) Beams 1 and 2 are failed in an s-shaped manner. (b) Beams 1 and 2 have been partially repaired by applying 20 Vpp to the actuation pad (beams are grounded), thus oscillating the beams and fully releasing them from the substrate. The frequencies applied ranged from 4 to 20.6 MHz. This excitation caused the failure mode to change from s-shaped to arc-shaped.

as a function of the dynamic excitation parameters. However, the remainder of this paper is intended to provide a theoretical foundation for understanding the dynamic stick-release process and to identify effective excitation parameters that can be used to guide future experiments and device design.

III. ANALYTICAL MODELS

Two models are developed to predict the initiation of decohesion of adhered cantilevers, which are subjected to harmonic point-loads or uniform pressures. The first model is a linear vibration model for the response of the beam (Section III-A). This model is used as an input to an interface fracture model (Section III-B), which yields the energy release rate governing debond initiation. These models are used together in Section IV to predict the onset of decohesion in terms a critical interface energy. Fig. 1(a) depicts the geometry analyzed here: a cantilevered microbeam deformed into an s-shape with adhesion at the beam-substrate interface. The rectangular beam has length L , an unstuck length s , depth b , and thickness h . Lastly, δ is the gap between the substrate and the neutral axis of the free standing beam. Two different harmonic loading scenarios are considered: a point load and a distributed load. The motivation for these two cases is as follows. The point load solution may be used, via a Green's function analysis, to examine more complicated pressure distributions. The distributed load approximates

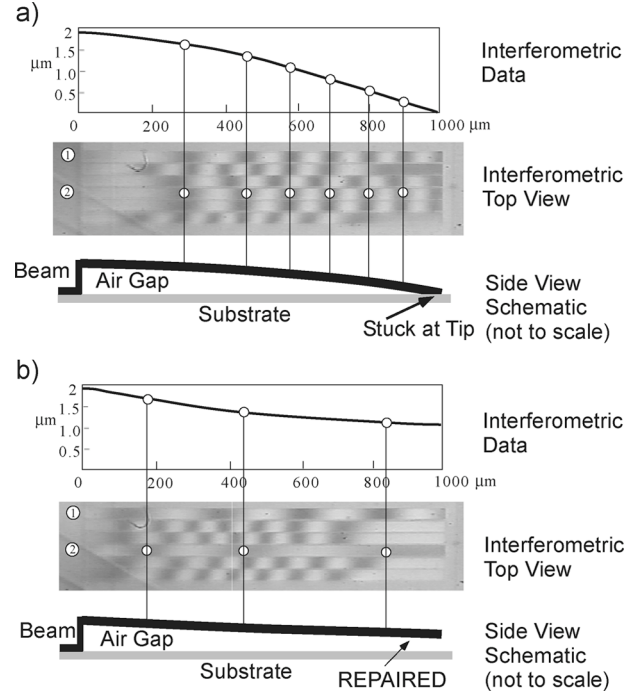


Fig. 3. (a) and (b) show the same set of beams (though different from Fig. 2). (a) Beams 1 and 2 are failed in an arc-shaped manner. (b) Beams 1 and 2 have been fully repaired by applying 220 Vpp to the actuation pad (beams are grounded), thus oscillating the beams and fully releasing them from the substrate. The frequencies applied ranged from 2.6 to 400 kHz.

the applied voltage used in the preliminary experiments of Section II. Of course, the applied voltage problem provides a force that is gap-dependent. However, with the actuation pad near the post, this effect can roughly be ignored since the deflection of the loaded portion of the beam is relatively small—making variations in the gap negligible.

A. Vibration Model

The stiction-failed cantilever beam shown in Fig. 1(a) is subjected to a harmonic transverse load. For an arbitrary load distribution, this may be expressed as

$$P(x, t) = P(x) [\cos(\Omega t) - 1]. \quad (1)$$

This consists of a static downward load and a periodic load. This form of excitation was chosen because upward forces are difficult to apply in either an electrical or mechanical loading scenario; the constant term ensures that the load never exceeds zero (i.e., it is always pushing down). In addition, the time-varying portion of this load gradually lifts off from zero (it has a zero slope at $t = 0$), as would most realistic loadings. Note that in the case of mechanical loading (as opposed to the electrical loading used in the stiction release experiments), this load might be delivered by, say, an instrumented nanoindenter.

We define the total deflection as a superposition of the no-load equilibrium position of the adhered beam (i.e., the s-shape) and the response of the beam under the load given by (1). The initial, zero-load s-shape of the beam $w_o(x)$ is measured from the straight, freestanding position. This initial shape is dictated by elementary beam theory and the following boundary conditions:

$w_o(0) = 0$, $w'_o(0) = 0$, $w_o(s) = \delta$, and $w'_o(s) = 0$. The initial deflection (with zero applied load) of the beam is

$$w_0(x) = \delta \left(3 \left(\frac{x}{s} \right)^2 - 2 \left(\frac{x}{s} \right)^3 \right) \quad (2)$$

where the unstuck length s may be determined using static fracture mechanics, as will be described in Section III-B. This shape is used as the reference position for the loaded beam, i.e., $w(x, t)$ is measured from $w_o(x)$. This loaded beam deflection includes inertial effects and the influence of the externally applied load. Modal analysis is used to obtain a solution to the governing dynamic beam equation, given by

$$m\ddot{w} + c\dot{w} + EIw''' = -P(x)[\cos(\Omega t) - 1] \quad (3)$$

where m is the mass per unit length, c is the structural damping constant, and EI is the bending rigidity; dots and primes refer to derivatives with respect to time and space, respectively. Note that $w(x, t)$ represents the deflection arising from the applied load and does not include the initial deflection arising from the gap separation. In other words, $w(x, t)$ is the solution to a straight, clamped-clamped beam of length s . A separable solution of the following form is sought:

$$w(x, t) = \sum_{i=1}^{\infty} A_i(t) \Psi_i(x) \quad (4)$$

where $\Psi_i(x)$ is the i th mode shape of a clamped-clamped beam [19]. Substituting this assumed solution into (3) and invoking orthogonality renders the following second-order ordinary differential equation for the i th modal amplitude $A_i(t)$:

$$\ddot{A}_i + 2\zeta_i \omega_i \dot{A}_i + \omega_i^2 A_i = p_i [1 - \cos(\Omega t)] \quad (5)$$

with $\omega_i^2 = EI\beta_i^4/m$, $p_i = \int_0^s (P(x)\Psi_i(x)/m)dx$, ζ_i the modal damping ratio, and β_i a constant arising from the i th mode shape [19]. Values for β_i are 4.73, 7.85, 10.99, etc., for first, second, and third mode, respectively. The complete solution to (5) consists of three parts obtained via superposition. A_i^p is the response due to the static downward load p_i . A_i^Ω is the steady-state response due to the harmonic load. A_i^t is the transient response. In this case, the lateral deflection, measured from $w_o(x)$, is

$$w(x, t) = \sum_{i=1}^{\infty} [A_i^p + A_i^\Omega + A_i^t] \Psi_i(x). \quad (6)$$

The individual terms are

$$A_i^p(t) = \frac{p_i}{\omega_i^2} \quad (7)$$

$$A_i^\Omega(t) = \frac{(-p_i/\omega_i^2)}{\left([1 - r^2(\omega_1/\omega_i)^2]^2 + [2\zeta r \omega_1/\omega_i]^2 \right)^{1/2}} \times \cos(\Omega t - \phi_i) \quad (8)$$

and

$$A_i^t(t) = e^{-2\zeta \omega_i t} [C_i^I \cos(\omega_i^d t) + C_i^{II} \sin(\omega_i^d t)]. \quad (9)$$

Here, $r = \Omega/\omega_1$ is the dimensionless driving frequency, $\omega_i^d = \omega_i \sqrt{1 - \zeta_i^2}$ is i th damped natural frequency, $\phi_i = \tan^{-1}((2\zeta_i r \omega_1/\omega_i)/(1 - r^2(\omega_1/\omega_i)^2))$ is the phase angle, and the coefficients C_i^I and C_i^{II} are found from the initial conditions. Throughout this paper, it is assumed that the initial conditions are zero displacement (relative to the static position $w_o(x)$) and zero velocity. In this case, the constants are

$$C_i^I = \frac{p_i}{\omega_i^2} \left[\frac{\cos(\phi_i)}{d} - 1 \right] \quad (10)$$

and

$$C_i^{II} = \frac{p_i}{\omega_i^2 \omega_i^d} \left[\zeta_i \omega_i \left(\frac{\cos(\phi_i)}{d} - 1 \right) + \frac{\Omega}{d} \sin(\phi_i) \right] \quad (11)$$

where $d = ([1 - r^2(\omega_1/\omega_i)^2]^2 + [2\zeta r \omega_1/\omega_i]^2)^{1/2}$.

In the following section, it will be clear that the energy release rate has two portions. The first stems from the initial deflection $w_o(x)$. The second comes from the dynamic bending moment per unit thickness at the crack tip ($x = s^-$). The latter quantity may be determined using the dynamic deflection (6) and the relation $M(s^-, t) = (EI/b)(d^2 w(s^-, t)/dx^2)$.

B. Fracture Model

A fracture mechanics model is used to predict the onset of decohesion between the beam and the fixed, semi-infinite substrate. The “crack tip” occurs at the point of separation of the two surfaces, as indicated in Fig. 1(a). The energy release rate G governs the propagation of the crack tip, which corresponds to growth of the unstuck region. Our loading scenario may be achieved by a *sequential* loading procedure. First, a prescribed displacement δ is applied to the right side of the beam (for $x \geq s$); this produces the initial s-shape deflection $w_o(x)$. Secondly, the prescribed force (1) is then applied to this new geometry. Each of these contribute to the overall energy release rate.

There are subtleties involved in calculating energy release rates for scenarios that involve both displacement and force loads [20]. Generally speaking, the energy release rates from two distinct loadings do not superpose; because $\sigma \propto K$ (the stress intensity factor) and $G \propto K^2$, it is evident that $G \neq G_1 + G_2$. However, when the deformation arising from the second load is referenced to the deformed state of the first, the situation is slightly different. Here, the prescribed displacement (corresponding to the gap separation) leads to G_1 . Next, the force is applied and the work is $W = \mathbf{F} \cdot \mathbf{d}$, where \mathbf{d} is the *additional* displacement produced after the initial, prescribed displacement. This approach has the effect of uncoupling the two processes, as described by Lawn [20]. Thus, the correct expression for G in this particular loading scenario is uncoupled: $G = K_1^2 + K_2^2 = G^1 + G^2$ —provided one uses the relative displacements arising from the pressure load.

To arrive at our initial geometry, the right side of the beam ($x \geq s$) must undergo a prescribed (vertical) displacement of δ . This leaves the beam in the s-shape, and the deformation is given by $w_o(x)$. This energy release rate, which represents a constant that is independent of the applied pressure or point loads, is given by

$$G_s = 18 \frac{EI\delta^2}{bs^4}. \quad (12)$$

See [3], [5], and [6]. The subscript s represents the “static” contribution for the energy release rate due to the initial static deflection of the beam. For a given interface energy Γ_i , this equation dictates the unstuck length $s = \sqrt[4]{18EI\delta^2/b\Gamma_i}$. This expression is obtained by striking a balance between the strain energy and the interface energy. In other words, $G = \Gamma_i$, which indicates an equilibrium configuration associated with impending debonding. Any upward load causing an upward deformation at the crack tip immediately initiates debonding.

The applied force (1) is introduced, and displacements are referenced to the deformed state arising from imposing (12). The energy release rate may be derived from an energy flux integral approach [21]. This includes strain energy, transverse inertial effects, and inertial effects arising from changes in the crack length s (i.e., crack propagation). The energy release rate is

$$G_d = \frac{6M^2(s^-, r, t)}{Eh^3} \left(1 - \frac{\dot{s}^2}{c_o^2} \right) \quad (13)$$

where \dot{s} is the rate of crack advance and c_o is the shear wave speed in the material [21]. $M(s^-, r, t)$ is the bending moment per unit depth that results from the applied force only. The subscript d indicates that this contribution to the energy release rate is due to the “dynamic” load. The moment due to the initial deformation $w_o(x)$ has been accounted for in the first part of the loading (the prescribed displacement). The objective here is to examine parameters that lead to the *initiation* of crack advance; hence, $\dot{s} = 0$. Note that a similar expression may be obtained using a purely static energy release rate along with the dynamic response, as described in the Appendix.

The total energy release rate for this sequential loading process of a prescribed displacement and then an external force is

$$G_{\text{tot}} = 18 \frac{EI\delta^2}{bs^4} + \frac{6M^2(s^-, r, t)}{Eh^3}. \quad (14)$$

The criterion for the initiation of crack propagation is $G_{\text{tot}} = \Gamma_i$, where Γ_i is the interface energy. In these interface problems, Γ_i plays the same role as the material toughness for traditional fracture problems.

If one assumes that the initial unstuck length is governed by the condition given as (12), then the system is initially at an unstable equilibrium; any loading that increases the gap size (by decreasing the deflection from the initial value $w_o(x)$)

will trigger decohesion. When inertia effects are neglected, no amount of electrostatic pressure, which acts to narrow the gap, will trigger decohesion. However, inertial effects will cause positive deflections (relative to the initial static equilibrium position) that increase the gap size and trigger debonding. That is, even compressive pressure can trigger decohesion because inertia effects will cause “overshoot” past the initial static deflection.

In fact, *any* dynamic loading, even at low frequencies, will trigger decohesion when (12) is imposed, i.e., when the initial unstuck length is determined from $G = \Gamma_i$. This is because even very low frequencies result in a finite, albeit asymptotically small, overshoot that raises the energy release rate above the initial value. It is clear from the preliminary experiments that a critical forcing amplitude and frequency combination is required to trigger decohesion. This can be rationalized physically as follows. The applied electrostatic pressure is compressive, and acts to close the gap. This initial squeezing of the gap leads to changes in the local details of the contact in the adhered region. It is likely (and supported by the experiments) that lateral sliding of asperities during initial compressive loading increases the true contact area. Since Γ_i will depend strongly on the conformational details of the contact [6], it is likely that Γ_i increases above the initial value that describes the initial adhesion event.

To capture this behavior, the interface energy that must be overcome in the vibration repair mechanism is $C\Gamma_i$, where C is a positive constant greater than unity. The modeling and dynamic repair experiments such as those outlined here represent an opportunity to determine experimentally the magnitude of this interface energy enhancement C .

IV. RESULTS

Two different loading scenarios are considered: a point force, as might be applied with an external probe [3], and a uniform pressure applied over a portion of the beam. For point forces, the load distribution is $P(x) = P\delta(x - x_o)$, where x_o is the load location and $\delta(x)$ is the Dirac delta function. While point loads may be difficult to implement at the microscale, they provide the foundation for more complicated distributed loading scenarios via a Green’s function analysis. The uniform pressure loading corresponds to $P(x) = P[H(x - x_1) - H(x - x_2)]$, where $H(x - x_i)$ is the Heavyside step function initiated at $x = x_i$. This scenario is motivated by the possibility of exciting the beam with harmonic electrostatic pressures, generated by varying the electrical potential between the beam and substrate over the region $x_1 < x < x_2$. Strictly speaking, an electrostatic pressure generated between the deflected beam and substrate would not be uniform, as it depends on the separation between the beam and the substrate. However, if the loading region is near the left post [see Fig. 1(a)], the deformations would be small and the variation in the gap size could be ignored.

The remainder of this paper focuses on finding parameter combinations of the excitation frequency (Ω) and applied force (P) that lead to the initiation of debonding. The former is normalized by the first natural frequency of the system: $r = \Omega/\omega_1$.

The latter is normalized by the load required to cause initial contact between the tip of a freestanding cantilever beam and a substrate: $\bar{P} = P/P_c$. For the point-loaded beam, the contact load is given as

$$P_c = \frac{2EI\delta}{x_0^2(L - (x_0/3))}. \quad (15)$$

For a uniformly distributed load over the region $x_1 < x < x_2$, the load per unit length required to initiate contact is

$$P_c = \frac{24EI\delta}{[x_1^3(4L - x_1) - x_2^3(4L - x_2)]}. \quad (16)$$

To put things in perspective, consider the following microcantilever [3]: $EI = 3.2 \times 10^{-12} \text{ N} \cdot \text{m}^2$, $d = 2 \mu\text{m}$, $b = 30 \mu\text{m}$, $h = 2 \mu\text{m}$, $L = 1000 \mu\text{m}$, $x_o = 0.25L = 250 \mu\text{m}$ (point force), $x_1 = 0$, and $x_2 = 0.2L = 200 \mu\text{m}$ (distributed force). In this case, the normalizing loads are $P_c = 3.08 \times 10^{-7} \text{ N}$ and $P_c = 5.05 \times 10^{-3} \text{ N/m}$ for the point and distributed forces, respectively.

A. Modal Convergence

Whenever a dynamic response is described in terms of a series solution [i.e., (4)], one must establish the number of modes required to obtain accurate results. For the remainder of this paper, the results are considered convergent if, near any resonance, additional modes do not change debonding force by more than $\Delta(P/P_c) < 0.01$. The focus is placed squarely on frequencies near resonance; the logic being that these frequencies hold the most promise for initiating debonding. However, it is important to recognize that this criterion does not automatically ensure that the behavior at any arbitrary frequency will be “as converged.” In other words, if N modes are required for convergence at $\Omega/\omega_1 = 2.7$ (the second resonance), then using N modes at $\Omega/\omega_1 = 4.0$ may or may not be sufficient to ensure that the required forcing amplitude is converged to within the criteria $\Delta(P/P_c) < 0.01$.

For a point force located at $x_o/s = 0.25$, two modes are sufficient to achieve the aforementioned convergence. For a uniformly distributed load applied over the range $0 < x/s < 0.2$, four modes have to be retained. However, for the sake of uniformity and to ensure satisfactory convergence at all frequencies, ten modes are retained for all of the results presented herein.

B. Results for Point-Loads

1) Behavior in the Steady-State Regime: In this section, debond initiation is examined using only the steady-state response, i.e., $A_i^t = 0$ in (6). There are three reasons for first looking at only the steady-state behavior. First, it is possible that some adhesion mechanisms are time or cycle-dependent: for example, adhesion arising from hydrocarbon contamination. In this case, debonding might require numerous successive cycles with a large driving force to damage the material accumulated at the interface. This is more likely to occur during the steady-state response than in the transient phase of the motion. Secondly, a steady-state only analysis is conservative. This stems from the fact that the total response is the sum of the transient and the

steady state. Using only the steady state will result in smaller amplitudes (in the transient phase of motion). Hence, larger forces will be required to produce sufficient deformation to induce debonding. Thirdly, a closed-form expression relating the force amplitude and the excitation frequency may be easily obtained. This allows for a straightforward estimate of the load amplitude needed to initiate debonding for a given excitation frequency.

The closed-form expression for the excitation amplitude (to produce debonding) as a function of excitation frequency is found using the energy release rate

$$G_{\text{tot}} = 18 \frac{EI\delta^2}{bs^4} \pm \frac{6[M_1 + M_2 + \dots]^2}{Eh^3} \quad (17)$$

where M_i is the contribution of the i^{th} mode to the moment at the crack tip. The maximum steady-state moment is simply

$$M_i = \frac{P EI}{k_i b} \frac{\Psi_i(x_o)\Psi_i''(s^-) \cos(\phi_i)}{\left([1 - r^2(\omega_1/\omega_i)^2]^2 + [2\zeta_i r \omega_1/\omega_i]^2\right)^{1/2}}. \quad (18)$$

If $D_i = ([1 - r^2(\omega_1/\omega_i)^2]^2 + [2\zeta_i r \omega_1/\omega_i]^2)^{1/2}$ and $z_i = \Psi_i(x_o)\Psi_i''(s^-) \cos(\phi_i)/(k_i D_i)$, then the steady-state energy release is given by

$$\begin{aligned} G_{\text{tot}} &= 18 \frac{EI\delta^2}{bs^4} \pm \frac{6}{Eh^3} \left[\frac{EI}{b} (Pz_1 + Pz_2 + \dots) \right]^2 \\ &= 18 \frac{EI\delta^2}{bs^4} \pm \frac{P^2 EI}{2b} \left[\sum_{i=1}^N z_i \right]^2. \end{aligned} \quad (19)$$

Applying the criterion for initiation of crack propagation, namely, that the energy release rate is equal to the new (compressed) interface energy $G = C\Gamma_i$, one obtains

$$C\Gamma_i - \frac{18\delta^2 EI}{bs^4} = \frac{P^2 EI}{2b} \left[\sum_{i=1}^N z_i \right]^2. \quad (20)$$

Solving for the load amplitude P yields

$$P = \sqrt{\left[C\Gamma_i - \frac{18\delta^2 EI}{bs^4}\right] \frac{2b}{EI(\sum z_i)^2}}. \quad (21)$$

For a given excitation frequency Ω/ω_1 (which appears in z_i), (21) may be used to determine the steady-state force amplitude required to initiate debonding.

Consider the steady-state response for a point-load located at $\xi_o = x_o/s = 0.25$ (the normalized location along the beam) with damping $\zeta_i = 0.01$. The solid line in Fig. 4 shows the steady-state (only) load amplitude required to initiate debonding as a function of the excitation frequency, i.e., the (Ω, P) parameter plane. At low frequencies, $\Omega/\omega_1 \rightarrow 0$, the excitation is driven to zero because $[\cos(\Omega t) - 1] = 0$; see (1); hence, the force amplitude $P(x)$ required to initiate peeling asymptotes to infinity, because the inertia terms that drive the beam past the

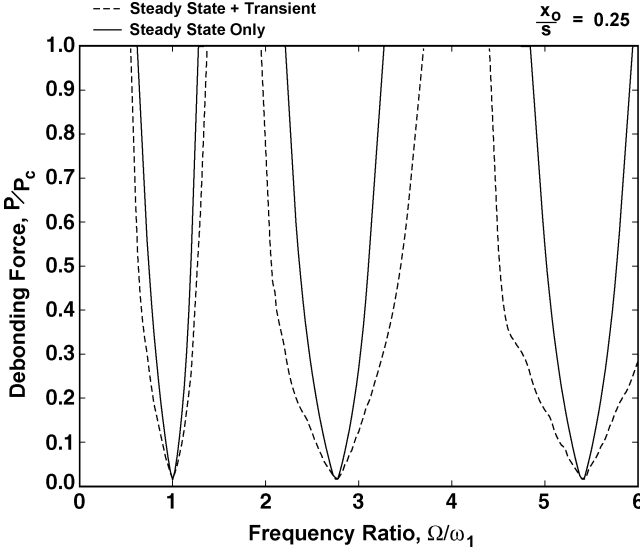


Fig. 4. A parameter diagram showing the combination of the applied point force and excitation frequency required to *initiate* debonding. Point load at $\xi = 0.25$, damping $\xi = 0.01$.

initial static deflection asymptotes to zero. As the frequency is increased from zero, inertial effects become increasingly important, and the required force amplitude decreases to a minimum at approximately $\Omega/\omega_1 = 1$. At resonance, the overshoot due to inertia effects is amplified and the added energy overcomes the interface energy and debonding is initiated at lower force levels. As the excitation frequency $r = \Omega/\omega_1$ is increased beyond the first resonance, the required force increases. This process is played out each time the excitation frequency approaches a natural frequency $\omega_1, \omega_2 = 2.76\omega_1, \omega_3 = 5.40\omega_1$, etc.

In between resonances, the required load amplitude increases dramatically. The physical mechanism at play is the modal phase difference ϕ_i between the excitation and the response. To demonstrate this, consider the power imparted to the system over one steady-state cycle. This is defined as the integral of the force multiplied by the load point velocity

$$\text{Power} = \int_0^{T=2\pi/\Omega} \left(P \cos(\Omega t) \sum \frac{\partial A_i^\Omega}{\partial t} \Psi_i(x_o) \right) dt. \quad (22)$$

For simplicity, one may ignore the constants and focus on the time-dependent terms $(\cos(\Omega t)\dot{A}_i^\Omega)$. Differentiating (8) gives \dot{A}_i^Ω . Noting that the modal phase angle ϕ_i transitions from zero below resonance, to $\pi/2$ at resonance, to π above resonance, the power integral becomes

$$\int_0^T \sin(\Omega t - \phi_i) \cos(\Omega t) dt = \begin{cases} 0, & \phi_i = 0 \\ \pi/2, & \phi_i = \frac{\pi}{2} \\ 0, & \phi_i = \pi \end{cases}. \quad (23)$$

This clearly indicates that away from the i th resonance, the power delivered to the system by the i th mode is virtually zero. At the i th resonance, the power delivered is a finite value. So in between resonant frequencies, very little power is delivered to the system and a much larger load amplitude is required to make

up for this power loss. Conversely, near $\Omega = \omega_i$, the power delivered by the i th mode is large and, although all of the other modes contribute almost nothing, the load required to initiate decohesion is reduced.

2) *Behavior in the Transient Regime:* Now consider the total beam response (steady-state + transient) and the energy release rate. In this case, a closed-form expression for the parameter combinations (Ω, P) that initiate peeling does not exist. Instead, a numerical procedure is used. The procedure involves fixing the excitation frequency, Ω/ω_1 and setting the excitation level, P/P_c to a low value. The total dynamic response is then used to calculate the time-dependent moment at the crack tip, such that the value of the energy release rate can be monitored as a function of time for, say, 1000 forcing cycles. If G_{tot} does not exceed $C\Gamma_i$, then the excitation amplitude is increased and the procedure is carried out again. This continues until a forcing amplitude is found such that $G_{\text{tot}} = C\Gamma_i$ for at least one instant in the response. This indicates that debond initiation has taken place at this (Ω, P) combination; this parameter combination is saved. The excitation frequency is incremented and the procedure is repeated.

Now consider the dashed lines in Fig. 4; these correspond to using the total response to calculate the energy release rate. The total solution results show the same general trends as the steady-state only results. At low frequencies, the required force amplitude is infinite. Near each resonant frequency, the force required to initiate debonding drops. And in between resonant frequencies, the required excitation amplitude increases. Quantitatively, the transient + steady-state results require a much lower amplitude than the steady state only case. This confirms the earlier statement that estimates based on a steady-state analysis are conservative.

3) *Anomalies:* The moral of the story is clear: drive the system near a resonant frequency and the likelihood of repair is high. However, this is not universally true. Consider, for example, an alternate load location, $\xi_o = 0.5$. Fig. 5 shows the (Ω, P) parameter combinations leading to decohesion. For clarity, only the steady-state results are shown, though the trends found with the transient analysis are exactly the same as in Section IV-B2. Most of the trends follow those of Fig. 4, for the case of $\xi_o = 0.25$. At low frequencies, the required force approaches infinity, and at the first and third natural frequencies, the required force drops nearly to zero. However, with this new load location, there is no drop near the second natural frequency. This occurs because the load location coincides with a vibration node for the second mode. The system is being forced to displace at its midpoint, though a purely second mode response cannot have a displacement at its midpoint. As a result, all of the energy (work) flows into the odd modes, which contribute little power to the system due to phase differences, as explained via (23). In fact, the steady-state only model predicts that an infinite force is required at the second resonant frequency $\Omega/\omega_1 = 2.76$. This behavior is an important consideration: if a point load drives a system at the i th natural frequency and is located at a node of the i th mode, no motion will be produced and desticking is unlikely. Of course, transients from other modes may initiate release but very high force levels would be required.

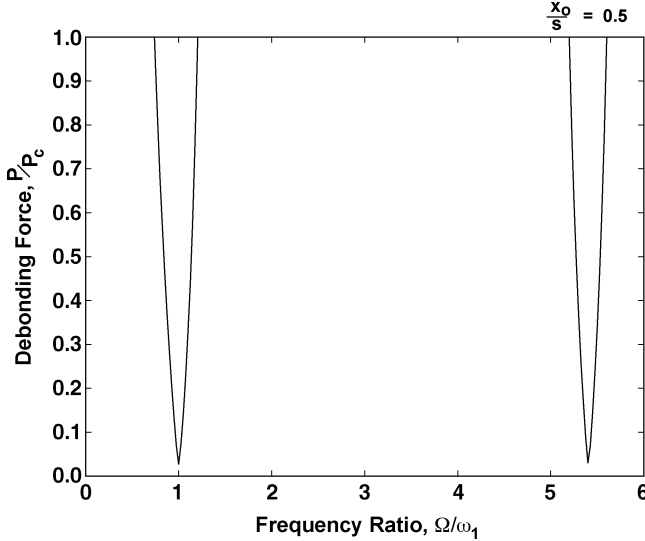


Fig. 5. A parameter diagram showing the combination of the applied point force and excitation frequency required to *initiate* debonding. Here the load is applied at the node of the second vibration mode (at the center of the beam), preventing debond initiation near the second resonance $\Omega/\omega_1 \approx 2.7$.

C. A Note on Damping

Throughout this paper, it has been assumed that the damping can be represented with a linear viscous model. Moreover, the results presented thus far are for a particular level of damping: $\zeta = 0.01$. Of course, the results will be a sensitive function of both the damping mechanism and the level of damping ζ . The two primary sources of damping in this system are structural (viscous) [22] and squeeze film damping [23]. The latter is nonlinear and arises from the air trapped between the beam and the substrate. This is particularly important near the crack tip where the Knudsen number may be large [24]. Nonetheless, throughout this paper, we maintain a simply linear, viscous damping model. This is justified by the fact that as one moves away from the crack tip, the Knudsen number should drop quickly. This implies that the squeeze film damping is a localized phenomenon that is probably not dominant. In addition, the simple viscous model permits closed-form solutions. These analytical solutions allow us to make direct connections between physical mechanisms and the response of the system. The level of damping has been fixed at $\zeta = 0.01$, which is an appropriate level of traditional structural damping. Other works [22], [23] suggest that a much larger damping value is physically reasonable in MEMS applications. But regardless, the specific value of damping ζ will only change the behavior quantitatively, not qualitatively (provided $\zeta < 1$).

This brief discussion of the assumptions underscores the need to obtain reliable experimental damping measurements for a particular device prior to using the vibration release technique proposed here. Such tests are currently being developed by the authors for the cantilevers described in Section II.

D. The Beam With a Uniformly Distributed Load

Fig. 6 shows the (Ω, P) parameter combinations leading to debond initiation for a uniformly distributed, harmonic excita-

tion over the range $0 < \xi < 0.2$. At low frequencies, the required force rises to infinity due to the compressive load. Again, the required load drops near the first resonant frequency. As the frequency is increased past resonance, the required force increases but drops again near the second and third resonant frequencies. This is altogether similar to the point load case.

Another anomaly may occur in this loading scenario. Consider applying a uniform load across the entire unstuck length $0 < \xi < 1$. Here, the load is being applied symmetrically about the midpoint. In this case, one should expect no drop in the required force near the second natural frequency. This occurs because the symmetric load cannot excite the asymmetric second mode. As a result, the second mode (or any asymmetric mode, for that matter) cannot be excited by this particular load distribution.

E. Minimum Required Force Amplitudes

Based on the results presented in Figs. 4–6, it is clearly advantageous to excite the system near a resonant frequency. Notable exceptions include driving the system near a vibration node or trying to excite asymmetric modes with symmetric load distributions (and vice versa). But in the absence of these unusual cases, an obvious question arises: is there a preferred resonant frequency? To answer this, focus on the steady-state solution. The dynamic moment at the crack tip, which drives the debonding, is

$$M = \sum_{i=1}^{\infty} \frac{p_i \Psi_i(x)}{D_i E I \beta_i^2} \sin(\Omega t - \phi_i). \quad (24)$$

The quantities $D_i = ([1 - r^2(\omega_1/\omega_i)^2]^2 + [2\zeta r \omega_1/\omega_i]^2)^{1/2}$ and β_i increase with successive modes. Thus for a fixed value of Ω , the term Ω/ω_i will decrease, causing D_i to increase simultaneously. β_i increase with " i ." So the denominator increases with successive resonances. Hence, at higher resonances, the contribution from the moment to G_t is smaller and debonding is less likely. Put another way, the amplitude of the steady-state moment will always decrease with each successive mode, thereby decreasing the energy fed to the crack tip, inhibiting the release of stiction failed beams. While there is a benefit to driving the system at any resonant frequency, exciting the component at its lowest (i.e., its fundamental) frequency yields the smallest forcing amplitudes and, hence, is optimal.

F. Numerical Subtleties

As indicated earlier, the number of modes required to assure a converged solution depends on the type of load and where it is applied on the structure. For cases where more modes are required (e.g., in excess of ten), certain subtle numerical difficulties can arise. Specifically, the higher beam modes depend sensitively on the number of significant digits retained in the constant parameters λ_i , κ_i , and β_i ; see [19]. At least double precision accuracy is required in λ_i , κ_i , and β_i to ensure that the higher mode shapes (through the fifteenth mode) satisfy the boundary conditions at the right end $x = s$. This is particularly important in this paper, since the crack resides at the right end of the beam (i.e., at $x = s$). If the appropriate boundary conditions are

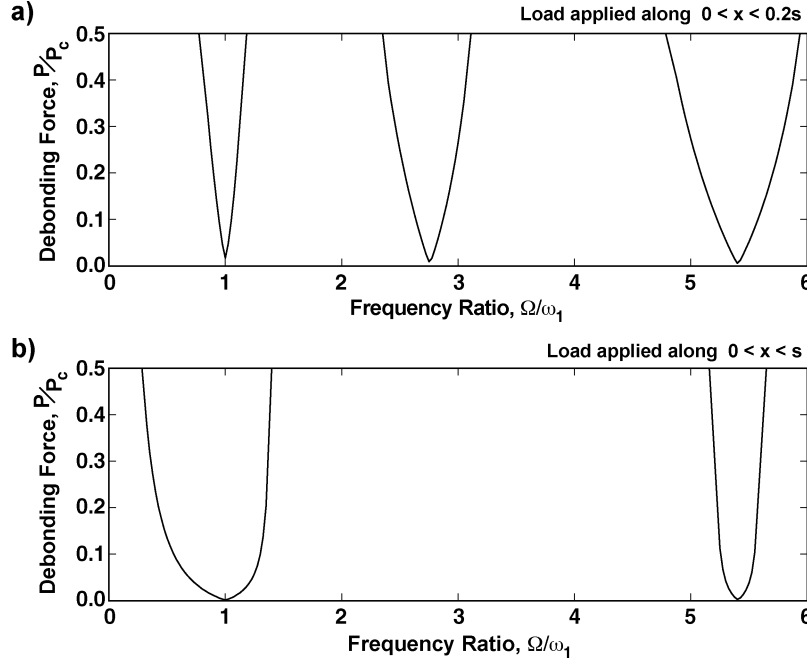


Fig. 6. Two parameter diagrams showing the combination of the applied distributed force and excitation frequency required to *initiate* debonding. (a) The load is applied over a portion of the beam and (b) the load is applied over the entire beam; symmetry prevents the second mode from being activated.

not enforced, the predicted force required for debonding will inevitably be wrong.

V. DISCUSSION

A. Experimental Evidence and Directional Dependence in Frequency Sweeps

The theoretical results presented in this paper suggest that structural vibrations may be used to achieve successful sticking repair of MEMS components. The fundamental mechanism driving this repair process is resonance. This is supported by the experimental results presented in Section II. The first set of tests involved an s-shaped beam with an initial unstuck length of approximately $900\ \mu\text{m}$. This has a corresponding first natural frequency of approximately $21\ \text{kHz}$ ($132\ \text{krad/s}$). The frequency underwent an increasing sweep from 2.6 to $400\ \text{kHz}$ with a load per unit length of approximately $0.1372\ \text{N/m}$. During this sweep through resonance, the beam partially unstuck from the substrate, i.e., the unstuck length s grew but total release was not achieved. The beam was then restuck, such that the unstuck length was again approximately $900\ \mu\text{m}$. Now a decreasing frequency sweep was applied from 400 to $2.6\ \text{kHz}$ at the same load level. Here complete repair was achieved. This repeatable direction dependence may be explained in terms of resonances. During the increasing sweep, partial repair was achieved by passing through the first resonance. The decreasing sweep is rather different. As the system passed through the fundamental resonance (near $21\ \text{kHz}$), debonding began, the unstuck length grew, and the fundamental frequency decreased ($\omega_i \propto 1/s^2$) to some new value $\omega^* < \omega_1$. As the downward sweep continued, the new fundamental resonance ω^* was encountered, permitting further peeling of the beam from the substrate. This process continued until total repair was achieved, as seen in Fig. 3(b).

A second set of tests were conducted in the megahertz range with a square wave. Only partial repair was achieved. If one takes a Fourier series view of the square wave, it is evident that numerous frequencies (beyond the dominant square wave frequency) are at play here. As a result, it is difficult to identify clearly whether a single resonance or a variety of resonances were responsible for this partial repair. However, this may be desirable; by intentionally using a square wave, the user spreads vibrational energy through various modes simultaneously. This increases the likelihood that at least one resonance will be encountered during a sweep.

B. Behavior at the Crack Tip: Crack Closing and Frictional Sliding

The analytical model (Section III-A) provides a physics-based framework for understanding the vibration release process. However, two pieces of physics were notably absent from this model: crack closure and frictional sliding.

As the beam is driven, it oscillates about the deformed (s-shaped) equilibrium position $w_o(x)$. During these oscillations, the material just to the left of the crack tip may contact the substrate. As such, the unstuck length s may vary between its equilibrium value, dictated by $G = C\Gamma_i$, and some shorter length, prescribed by the amplitude of the oscillation. This behavior is not accounted for in the present model. The following argument demonstrates that this change in the unstuck length is small and, as a result, may be ignored without significantly affecting the results. The change in s will scale with the response amplitude, which is amplified near resonance. So conceivably this effect will be most pronounced near resonance. So consider the resonant condition $\Omega/\omega_1 = 1.0$. Using just the first mode, the response amplitude (the maximum deformation) is superposed on the equilibrium position $w_o(x)$. The result is shown in Fig. 7. This clearly shows that a portion of the beam would have

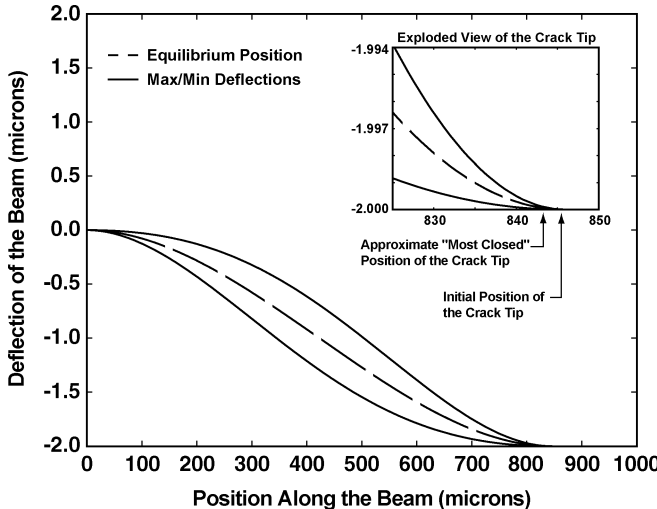


Fig. 7. A diagram showing the spatial envelope of the motion at resonance (equilibrium given by the dashed line). The inset clearly shows that the relative amount of crack closure during vibration is small ($\Delta s/s \approx 0.005$).

to be compressed into the substrate (though the model does not account for the reaction force back on the beam). It is critical to note that this region is very small and spans approximately $0.995 < x/s < 1$. In short, this is limited to 0.5% of the beam's length. If larger vibrations occurred, one might have to begin accounting for this contact with the substrate.

Another physical mechanism not described here involves frictional slippage at the interface. Throughout this paper, it has been assumed that mode I crack propagation (peeling of the beam from the substrate) is the dominant physical mechanism. However, it is possible that mode II crack propagation may occur; this corresponds to relative sliding between the two contacting surfaces. Mode II slipping is apt to occur if the beam is subject to a sizeable uniform axial load. Previous analyses of stiction-failed cantilevers have demonstrated that axially, loads arising from nonlinear coupling between vertical and horizontal displacements are relatively small [4]. More significant axial loads are generated at elevated temperatures. In this case, the axial stress promotes slip at the contact interface. In a recent study using beams similar to the ones considered here, thermal buckling occurred prior to observable slip [16]. This experimental observation supports the notion that mode I crack advance is the dominant mechanism. While the crack tip stress distribution undoubtedly involves mode II components, previous success with a mode-independent interface energy implies there is little evidence that a mixed-mode fracture approach is necessary to predict failure. This is a consequence of i) the mode I component being larger due to out-of-plane deflection and ii) the toughness increasing significantly with mode-mixity.

VI. CONCLUDING REMARKS

This paper explores a novel approach to stiction release using a beam vibration model in conjunction with a dynamic fracture model. This coupled model is then used to make predictions about what parameter combinations lead to the initiation of decohesion, where the beam begins to peel off of the substrate.

Using this model, critical combinations of the excitation frequency and force level (Ω, P), which initiate debonding, have been identified. It is clearly demonstrated that when the excitation frequency is near any natural frequencies of the adhered beam, the required force is reduced significantly. However, there are distinct regions in between the resonant frequencies where a harmonic excitation may be less effective than a static force (pulling on the beam). The cause of this behavior is the phase response of the system; in between resonances the response is either in-phase or 180° out-of-phase with the excitation. As a result, minimal power is delivered to the beam to initiate the decohesion process.

Also, the presence of vibration nodes limits the effectiveness of this method of release. For example, if a harmonic point load is applied at $\Omega = \omega_i$, the load location must not correspond to a node in the i th mode. This would result in no steady-state motion at the load point, which would inhibit the peeling process. Of course, transient behavior may still be sufficient to initiate peeling. Finally, though excitation near any resonant frequency reduces the force required to initiate decohesion, it is also shown that this benefit decreases at higher frequencies. This implies it is best to excite the system near its fundamental (lowest) natural frequency.

APPENDIX

The static energy release rate is defined by

$$G_s = \frac{1}{b} \frac{\partial U}{\partial s}$$

where b is the width of the beam and U is the strain energy. The latter term comes directly from Euler-Bernoulli beam theory

$$U = \frac{1}{2EI} \int_0^s [bM(x,t)]^2 dx.$$

So to evaluate the energy release rate, one must integrate the moment (obtained from the lateral deflection $w(x)$) and then differentiate the strain energy. Instead of carrying out these two steps, the fundamental theorem of calculus may be used. This says that if $f(x) = \int_a^x F(t)dt$, then $f'(x) = (d/dx)(\int_a^x F(t)dt) = F(x)$. Using this with our two above equations gives

$$G_s = \frac{1}{b} \left[\frac{b^2}{2EI} M^2(s,t) \right] = \frac{6M^2(s,t)}{Eh^3}$$

which is exactly the same expression as the second term in (14) for the zero crack speed case ($\dot{s} = 0$).

REFERENCES

- [1] R. Maboudian and R. T. Howe, "Critical review: Adhesion in surface micromechanical structures," *J. Vac. Sci. Technol.*, vol. 15, no. 1, pp. 1–20, 1996.
- [2] W. M. van Spengen, "MEMS reliability from a failure mechanisms perspective," *Microelectron. Reliab.*, vol. 43, no. 7, pp. 1049–1060, 2003.

- [3] E. E. Jones, M. R. Begley, and K. D. Murphy, "Adhesion of micro-cantilevers subjected to mechanical point loading: modeling and experiments," *J. Mech. Phys. Solids*, vol. 51, pp. 1601–1622, 2003.
- [4] E. E. Jones, K. D. Murphy, and M. R. Begley, "Adhesion of micro-cantilevers subjected to mechanical point loading: modeling and experiments," *Exper. Mech.*, vol. 43, no. 3, pp. 280–288, 2003.
- [5] C. H. Mastrangelo and C. H. Hsu, "A simple experimental technique for the measurement of the work of adhesion of microstructures," in *5th Tech. Dig. IEEE Solid State Sens. Actuators Workshop*, 1992, pp. 208–212.
- [6] M. P. de Boer, J. A. Knapp, T. A. Michalske, U. Srinivasan, and R. Maboudian, "Adhesion hysteresis of silicane coated microcantilevers," *Acta Mater.*, vol. 48, pp. 4531–4541, 2000.
- [7] Z. C. Leseman, S. Koppaka, and T. J. Mackin, "A fracture mechanics description of stress wave repair in stiction-failed microcantilevers: Theory and experiments," *J. Microelectromech. Syst.*, to be published.
- [8] Z. C. Leseman, S. Carlson, and T. J. Mackin, "Experimental measurements of the strain energy release rate for stiction-failed microcantilevers using a single-cantilever beam peel test," *J. Microelectromech. Syst.*, to be published.
- [9] N. Fujitsuka and J. Sakata, "A new processing technique to prevent stiction using silicon selective etching for SOI-MEMS," *Sens. Actuators A, Phys.*, vol. 97–98, pp. 716–719, 2002.
- [10] W. R. Ashurst, C. Yau, C. Carraro, C. Lee, G. J. Kluth, T. R. Howe, and R. Maboudian, "Alkene based monolayer films as anti-stiction coatings for polysilicon MEMS," *Sens. Actuators A, Phys.*, vol. 91, no. 3, pp. 239–248, 2001.
- [11] V. Kaajakari and A. Lal, "Pulsed ultrasonic release and assembly of micromachines," in *Proc. 10th Int. Conf. Solid-State Sens. Actuators*, 1999, pp. 212–215.
- [12] V. Kaajakari, S. Rodgers, and A. Lal, "Ultrasonically driven surface micromachined motor," in *Proc. 13th Int. Workshop Micro-Electro Mech. Syst.*, 2000, pp. 40–45.
- [13] N. C. Tien, S. Jeong, L. M. Phinney, K. Fushinobu, and J. Bokor, "Surface adhesion reduction in silicon microstructures using femtosecond laser pulses," *Appl. Phys. Lett.*, vol. 66, no. 2, pp. 197–199, 1995.
- [14] K. Fushinobu, L. M. Phinney, and N. C. Tien, "Ultrashort-pulse laser heating of silicon to reduce microstructure adhesion," *Int. J. Heat Mass Transfer*, vol. 39, no. 15, pp. 3181–3186, 1996.
- [15] L. M. Phinney and J. W. Rogers, "Pulsed laser repair of adhered surface—Micromachined polycrystalline silicon cantilevers," *J. Adhes. Sci. Technol.*, vol. 17, no. 4, pp. 603–622, 2003.
- [16] J. W. Rogers, T. J. Mackin, and L. M. Phinney, "A thermomechanical model of adhesion reduction for MEMS cantilevers," *J. Microelectromech. Syst.*, vol. 11, no. 5, pp. 512–520, 2002.
- [17] J. J. Sniegowski and M. P. de Boer, "IC-compatible polysilicon surface micromachining," in *Annu. Rev. Mater. Sci.*, 2000, vol. 30, pp. 299–333.
- [18] J. W. Rogers and L. M. Phinney, "Process yields for laser repair of aged, stiction-failed MEMS devices," *J. Microelectromech. Syst.*, vol. 10, pp. 280–285, 2001.
- [19] C. T. Chang and R. C. Craig, "Normal modes of uniform beams," *J. Eng. Mech. Div. ASCE*, pp. 1027–1031, 1969.
- [20] B. Lawn, *Fracture of Brittle Solids*. Cambridge, U.K.: Cambridge Univ. Press, 1993.
- [21] L. B. Freund, *Dynamic Fracture Mechanics*. Cambridge, U.K.: Cambridge Univ. Press, 1990.
- [22] Y. Cho, P. A. Pisano, and T. R. Howe, "Viscous damping model for laterally oscillating microstructures," *J. Microelectromech. Syst.*, vol. 3, no. 2, pp. 81–87, 1994.
- [23] J. M. Huang, K. M. Liew, C. H. Wong, S. Rajendran, M. J. Tan, and Q. A. Liu, "Mechanical design and optimization of capacitive micromachined switch," *Sens. Actuators A*, vol. 93, pp. 273–285, 2001.
- [24] R. P. Larose and K. D. Murphy, "Impact dynamics of MEMS switches," *Sens. Actuators*, submitted for publication.



Amit A. Savkar received the B.E. degree from the University of Mumbai (Bombay), India, in 1998. He is currently working towards the Ph.D. degree in the Department of Mechanical Engineering at the University of Connecticut, Storrs.

His research interest includes the application of vibrations and fracture mechanics to MEMS. He has been working on the stiction repair process of MEMS cantilever beams using vibrations.



Kevin D. Murphy is an Associate Professor in the Department of Mechanical Engineering at the University of Connecticut. His research interests include nonlinear dynamics, vibrations, stability and solid mechanics.



Zayd C. Leseman (S'06–M'07) received the B.S. and M.S. degrees from the Department of Mechanical and Industrial Engineering at the University of Illinois at Urbana-Champaign (UIUC) in 1997 and 2000, respectively. After receiving the M.S. degree, he started his own company in which he designed, fabricated, and patented a novel inkjet printhead. Upon conclusion of his entrepreneurial adventure, he returned to UIUC and completed the Ph.D. degree in May 2006.

Currently, he is an Assistant Professor of Mechanical Engineering at The University of New Mexico, Albuquerque. His research encompasses the design, fabrication, and analysis of novel MEMS/NEMS devices and experiments in order to study the surface, mechanical, and electrical properties of materials at the nanoscale. Additionally, he creates bioMEMS devices to perform studies in single-cell mechanics and nano/microfluidics.

Dr. Leseman is a Student Member of the American Society of Mechanical Engineers (ASME).

Thomas J. Mackin (M'97) received the Ph.D. degree in engineering science and mechanics from Pennsylvania State University, University Park, in 1991, where he utilized fractal geometry to develop new methods of analyzing the failure of ceramic materials.

He is Professor and Chair of the Department of Mechanical Engineering at the California Polytechnic and State University in San Luis, Obispo, CA. From 1993 to 2005, he was an Assistant, and then Associate Professor of Mechanical Engineering at the University of Illinois at Urbana-Champaign. In 2004, he became Director of the Illinois Homeland Security Research Center, and an affiliate of the Arms Control, Disarmament and International Security program. From 2002 to 2003, he served as an ASME Executive Office Fellow at the White House Office of Science and Technology Policy where he worked as a technology policy analyst and White House Liaison to the National Nanotechnology Initiative. From 1991 to 1993, he worked as a research engineer in the Materials Department at the University of California at Santa Barbara developing micromechanical models and test methods for composite materials. After three years at the University of California at Santa Barbara, he joined the Mechanical and Industrial Engineering Department at the University of Illinois. His current research interests include developing new methods for quantifying damage and predicting the service lifetime of aircraft composites, the development of new scientific tools for measuring stress in microelectronic packaging, MEMS, NEMS, and ferroelectrics, and research into functionalized nanostructures for applications as sensors and detectors.

Dr. Mackin is a Member of the American Society of Mechanical Engineers (ASME).



Matthew R. Begley received the B.S. and M.S. degrees in from the Pennsylvania State University, University Park, and the Ph.D. degree from the University of California at Santa Barbara.

Currently, he is an Associate Professor of Mechanical Engineering at the University of Virginia. His research has blended the mechanics underlying of material science with that controlling microdevice performance. Examples include studies of: the impact of compliant low-k materials on microprocessor reliability, the role of scale-dependent plasticity in hydrogen-assisted crack growth in metals, the mechanics of nanoporous metals, and chemomechanical sensors.